applied sciences

MDPI

Article

Assessment of MicroPET Image Quality Based on Reconstruction Methods and Post-Filtering

Hyeon-Sik Kim [1], Byeong-il Lee [2] and Jae-Sung Ahn [1,*]

[1] Medical Photonics Research Center, Korea Photonics Technology Institute, Gwangju 61007, Korea; knkc1120@kopti.re.kr
[2] Department of Smart Healthcare, Pukyoung National University, Busan 48513, Korea; bilee@pknu.ac.kr
* Correspondence: jaesung.ahn@kopti.re.kr

Abstract: The accuracy of positron emission tomography (PET) imaging is hampered by the partial volume effect (PVE), which causes image blurring and sampling. The PVE produces spillover phenomena, making PET analysis difficult. Generally, the PVE values vary based on reconstruction methods and filtering. Thus, selection of the proper reconstruction and filtering method can ensure accurate and high-quality PET images. This study compared the values of factors (recovery coefficient (RC), uniformity, and spillover ratio (SOR)) associated with different reconstruction and post-filtering methods using a mouse image quality phantom (NEMA NU 4), and we present an effective approach for microPET images. The PET images were obtained using a microPET scanner (Inveon, Siemens Medical Solutions, Malvern, PA, USA). PET data were reconstructed and/or post-filtered. For tumors smaller than 3 mm, iterative reconstruction methods provided better image quality. For tumor sizes bigger than 3 mm, reconstruction methods without post-filtering showed better results.

Keywords: mouse image quality phantom; reconstruction; post-filtering; image quality; PET performance

Citation: Kim, H.-S.; Lee, B.-i.; Ahn, J.-S. Assessment of MicroPET Image Quality Based on Reconstruction Methods and Post-Filtering. *Appl. Sci.* **2021**, *11*, 8707. https://doi.org/10.3390/app11188707

Academic Editor: Cecilia Di Ruberto

Received: 26 August 2021
Accepted: 15 September 2021
Published: 18 September 2021

1. Introduction

As a nuclear medicine functional imaging technique, positron emission tomography (PET) imaging is a powerful tool for diagnosis of tumor or cardiac function based on the estimation of metabolic processes. Unfortunately, the image accuracy of PET is relatively lower than that of other clinical imaging techniques such as magnetic resonance imaging (MRI) and computed tomography (CT) due to the intrinsic poor spatial resolution associated with the PET signal capturing principle. A physical solution is the development of gamma ray detectors (scintillator crystal) or signal processing circuits to correct for time of flight. Physical solutions are expensive and take a long time. We suggest an image correction method based on assessment of performance. Poor spatial resolution causes a partial volume effect (PVE) [1–3]. The accuracy of a PET image is affected by the PVE, resulting in image blurring and image sampling. Spill-in and spill-out (i.e., spillover) phenomena are generated by the PVE. The radioactivity of tissue may be underestimated due to spill-in from adjacent high-radioactivity tissue (e.g., tumor) [4]. The radioactivity of a volume of interest (VOI) may be overestimated due to spillover occurring into the VOI from high-radioactivity tissue (e.g., heart cavity). When analyzing cardiac perfusion in dynamic cardiac PET images, perfusion values change with time sequencing. The time–activity curve (TAC) peak of the myocardium is observed at full blood pool. However, the blood pool activity is maintained at a constant level from activity uptake in the myocardium, implying that the TAC of blood pool and myocardium is distorted by spillover and may need correction. Therefore, spillover creates difficulties in measuring myocardial blood flow (MBF) in cardiac PET analysis. The spillover phenomenon needs to be corrected using a recovery coefficient (RC). The RC value may be used in absolute measurement of myocardial blood flow (MBF) [5].

The RC, uniformity, and spillover ratio (SOR) of PET images are measured and assessed using the NEMA NU-4 phantom [6–10]. Soret et al. introduced a simple PVE correction method in which the measured uptake value in the region of interest (ROI) was divided by a correction factor, RC. For smaller tumors, tumor uptake value may be underestimated due to the PVE, and this problem is addressed by RC adaption. The spillover effect observed in myocardium from blood pool may distort the time–activity curve (TAC) in myocardium upon cardiac PET imaging. The distortion of the TAC affects the measurement of MBF and needs correction. The myocardial TAC may be corrected using the RC because of myocardial thinning.

Moreover, reconstruction methods have been developed and assessed for enhancement of PET image accuracy [11–14]. The PVE is depended on PET image reconstruction methods. Various PET image reconstruction methods have been evaluated in PET studies and classified into analytical and iterative approaches. Analytical approaches include filtered back projection (FBP), Fourier rebinning (FORE), and three-dimensional reprojection (3DRP). The iterative approaches include two- or three-dimensional ordered-subsets expectation maximization (OSEM2D or OSEM3D) and maximum likelihood expectation maximization (ML-EM) algorithms. Another study reported that an iterative reconstruction method was more accurate than analytical reconstruction methods for the absolute measurement of MBF [15]. Sondergaard HM et al. reported that the OSEM reconstruction method produced better image quality and less noise than the FBP reconstruction method [16]. HS Kim et al. compared reconstruction methods (FBP, OSEM2D, OSEM3D, and 3DRP) in cardiac PET imaging and reported that the OSEM3D reconstruction method showed a higher correlation with TTC staining and provided better image quality and contrast than other methods [17]. Post-filtering produces blurred images but can reduce the image noise. A filtering size larger than the image pixel size may result in image distortion. The selection of a suitable filter size can reduce the image noise and improve the image uniformity.

We executed performance assessment of microPET imaging using a mouse image quality phantom. The acquired phantom data were reconstructed using various reconstruction methods and filtered using a Gaussian filter. The accuracy of PET imaging is hampered by the PVE. The PVE is dependent on reconstruction methods and the selection of a valid reconstruction method can enhance the accuracy and the quality of PET images. In this report, we compared the values of factors (RC, uniformity, and SOR) between reconstruction methods and post-filtering and present a valid reconstruction method for microPET imaging to enable the selection of a reconstruction, post-filtering, and activity correction method for image analysis.

2. Materials and Methods

2.1. MicroPET, Reconstruction, and Post-Filtering

The PET images were obtained using a microPET scanner (Inveon, Siemens Medical Solutions, Malvern, PA, USA) with 20 × 20 lutetium oxyorthosilicate (LSO) crystals (each measuring 1.5 × 1.5 × 10 mm^3). The system comprised 64 detector blocks arranged in four contiguous rings with a diameter of 16.1 cm, a transaxial field of view (FOV) of 10 cm, and an axial FOV of 12.7 cm. Acquired data were sorted into 3D sinograms or directly into 2D sinograms. The 3D sinograms were then rebinned using FORE algorithm. The acquired 3D sinograms were reconstructed in 2D using the FBP and OSEM2D algorithms and in 3D using the OSEM3D and 3DRP algorithms.

PET data were reconstructed using FBP, 2 and 3D OSEM (OSEM2D and OSEM3D, respectively), and the 3DRP algorithm. In the FBP and OSEM reconstruction methods, a projection filter was fixed to a Ramp filter (cutoff at Nyquist frequency). A Hann filter (projection filter) was used only in the 3DRP reconstruction method. In the OSEM reconstruction methods, subsets were fixed to 16, and iteration numbers were 4, 6, and 8. The projection cutoff (0.5) was equally applied to all reconstruction methods. We measured the average reconstruction time per frame. The reconstructed images were filtered using a

Gaussian smooth 3D filter. The three Gaussian smooth 3D filters were set on a full width at half maximum (FWHM) sizes of 1, 2, and 4 mm. A total 36 images were generated as FBP, OSEM2D_I4, OSEM2D_I6, OSEM2D_I8, OSEM3D_I4, OSEM3D_I6, OSEM3D_I8, 3DRP_non, and 3DRP_Hann (multiplied by the four Gaussian filters).

2.2. Phantom Imaging and Measurement Methods

A mouse image quality phantom (NEMA NU-4) offered image resolution, uniformity, and contrast information for microPET imaging. The NEMA NU-4 image was acquired for 20 min with a 3.7 MBq (100 uCi) ^{18}F solution. In the phantom image, microPET performance was assessed via image accuracy, RC, uniformity, and SOR values. The resolution portion contains hot rods of 5, 4, 3, 2, and 1 mm diameter in a cold background for evaluating contrast resolution. The contrast portion contains water- and air-filled cylinders of 8 mm diameter in a hot background for evaluating accuracy of attenuation and scatter corrections. The uniformity portion contains a hot background with no structures for evaluating noise and nonuniformity artifacts.

The image accuracy was measured with a full width at half maximum (FWHM) of 5 fillable rods in the resolution area. Five fillable rods were used to determine the *RC*, defined as the ratio of the measured activity concentration in the rods and the activity concentration measured in the uniform area (UA).

$$Recovery\ Coefficient\ (RC) = \frac{Rod_{max}}{UA_{mean}} \quad (1)$$

where Rod_{max} is the maximum value of rods and UA_{mean} is the mean of uniformity area.

The fillable uniform area of the phantom was used to measure the *uniformity* as a measure of noise. A lower *%SD* indicated a lower variability in the dataset. Equally, a higher *%SD* showed that the dataset exhibited variations.

$$\%SD = \frac{UA_{sd}}{UA_{mean}} \times 100\ (\%) \quad (2)$$

where UA_{sd} is the standard deviation of uniform area.

The *SOR* of water- or air-filled area was calculated as follows:

$$Spillover\ Ratio\ (SOR) = \frac{WA_{mean}\ or\ AA_{mean}}{UA_{mean}} \quad (3)$$

where WA_{mean} or AA_{mean} are the mean of water or air area.

A circle ROI with a 2.5 mm radius was drawn in a hot rod of 5 mm diameter for calculation of peak signal-to-noise ratio (*PSNR*). The peak signal (*PS*) and mean square error (*MSE*) were measured in ROI. The PSNR was calculated as follows:

$$Peak\ signal - to - noise\ ratio\ (PSNR) = 10 \times \log_{10} \frac{PS^2}{MSE}\ (dB) \quad (4)$$

2.3. Image Analysis and Statistics

PMOD version 3.310 (PMOD Technologies Ltd., Zurich, Switzerland) and ImageJ 1.48v were used for image analysis. For assessing image accuracy, rod size was calculated from a line-profile list obtained using ImageJ. Image accuracy was compared via the size of five fillable rods, calculated using the FWHM method in the hot rod section. Image uniformity was compared using %SD values obtained from average and standard deviation in uniform area. The average and standard deviation values were measured across 10 regions of interest (ROIs, circles with a radius of 8 mm) drawn in a uniform area. The SOR values were calculated using mean of uniform area (voxel of interest, VOI) and mean of water or air area (VOI). In the phantom image, mean of uniformity area, standard deviation, and maximum value of rods were obtained using PMOD. The recovery coefficient and %SD were calculated using Equations (1) and (2).

3. Results

3.1. Image Accuracy

Phantom images are shown in Figure 1A. Image quality, sharpness, accuracy, and intensity were different following the reconstruction methods. We confirmed the image accuracy of reconstruction methods in hot rods of 5, 4, 3, and 2 mm diameter for the NEMA NU 4 mouse image quality phantom (Figure 1B). In the image, the rod size was measured as FWHM. In 2, 3, and 4 mm rods, the OSEM2D reconstruction method showed the highest accuracy among all tested methods. The accuracy of OSEM3D in the 2 mm rod was higher than that in other rods. In the 5 mm rod, 3DRP with Hann filter was the most accurate reconstruction method. In the iterative reconstruction methods (OSEM2D and OSEM3D), the measured rod size followed the number of iterations and was not changed by the specific pattern.

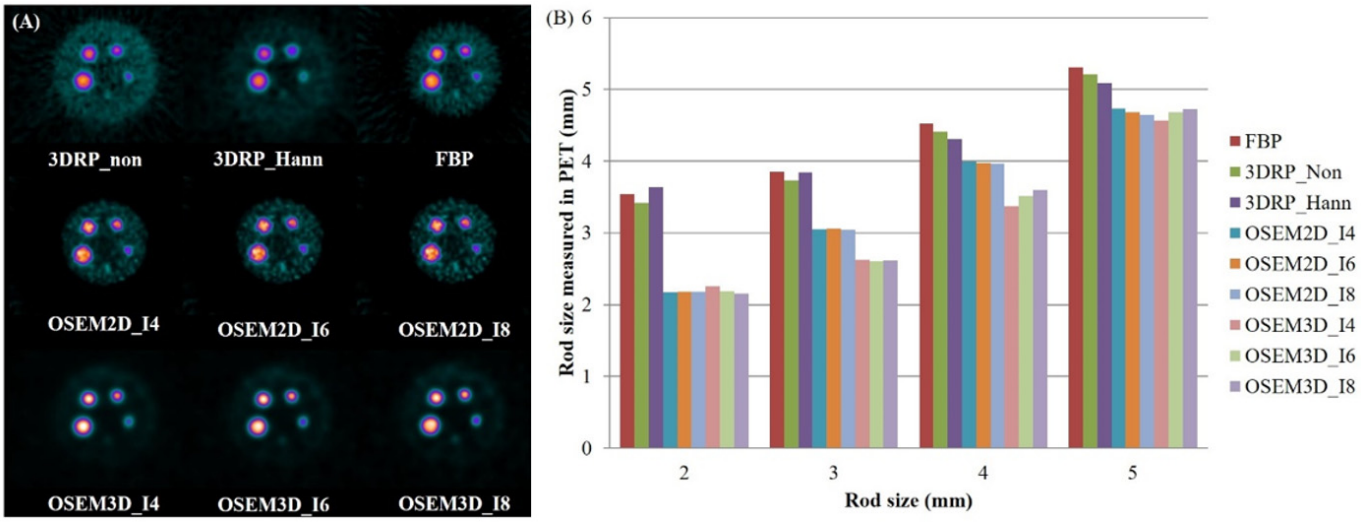

Figure 1. (**A**) Images of the hot rods in NEMA NU-4 were acquired via Inveon microPET. PET data were reconstructed using filtered back-projection (FBP), 2- and 3-dimensional ordered-subset expectation maximization (OSEM2D and OSEM3D, respectively), and 3-dimensional reprojection (3DRP). A Hann filter (projection filter) was used for the 3DRP reconstruction method only. In the OSEM reconstruction methods, iteration numbers were 4, 6, and 8. Image scale was fixed to the same scale. (**B**) The rod size was calculated via full width at half maximum in the NEMA NU-4 mouse image quality phantom. In the 2, 3, and 4 mm rods, the accuracy of OSEM2D reconstruction method was higher than that of the other methods.

3.2. Recovery Coefficient (RC)

The RC values were obtained for five hot rods of the NEMA NU-4. The RC value is theoretically limited between 1 and 0. The RC values of FBP and 3DRP without filtering were similarly obtained from published data (Figure 2A). However, the RC values of 3DRP with Hann filtering were lower than those of FBP and 3DRP without the filtering. The RC values were overcompensated in the iterative reconstruction methods (black lines in Figure 2A). We additionally confirmed that RC values varied with post-filtering (Figure 2B). The RC curve trend in OSEM reconstruction methods with a 2 mm Gaussian filtering was similar to that in the FBP reconstruction (dotted lines in Figure 2B).

3.3. Image Uniformity

The uniformity of the 3DRP and OSEM3D reconstruction methods was higher than that of FBP reconstruction method. However, the uniformity of the OSEM2D reconstruction method was lower than that of the FBP reconstruction method. In iterative reconstruction methods (OSEM2D and OSEM3D), image uniformity decreased with increasing number of iterations (Figure 3A). The uniformity values of OSEM2D_I4, I6, and I8 were 8.25, 9.84, and 11.18%, respectively. However, the increase in the range of uniformity in OSEM3D was lower than that in OSEM2D. The uniformity values of OSEM3D_I4, I6, and I8 were

6.03, 6.20, and 6.40%, respectively. We confirmed the effect of post-Gaussian filtering in iterative reconstruction methods (Figure 3B). The image uniformity was increased with the use of a Gaussian filter of 1 or 2 mm and decreased with a 4 mm Gaussian filter. Specifically, the image uniformity in the OSEM3D reconstruction method without Gaussian filtering was higher than that with the 4 mm Gaussian filter.

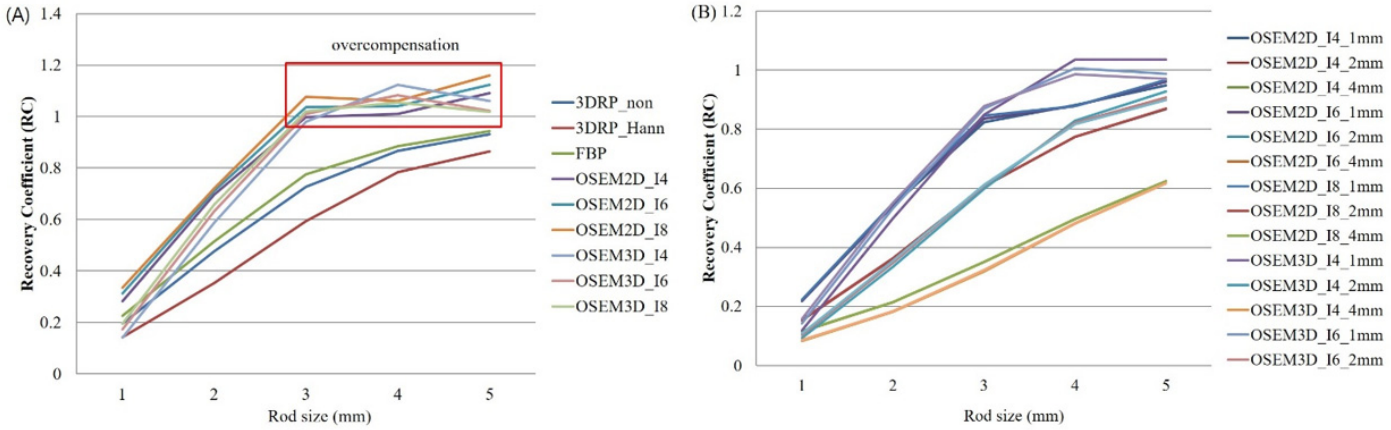

Figure 2. The RC values were obtained for five hot rods of the NEMA NU-4 mouse image quality phantom. (**A**) The RC values were overcompensated in iterative reconstruction methods (black lines). (**B**) The RC curve trend in the iterative reconstruction methods with 2 mm Gaussian filtering was similar to that in the FBP reconstruction (dotted lines).

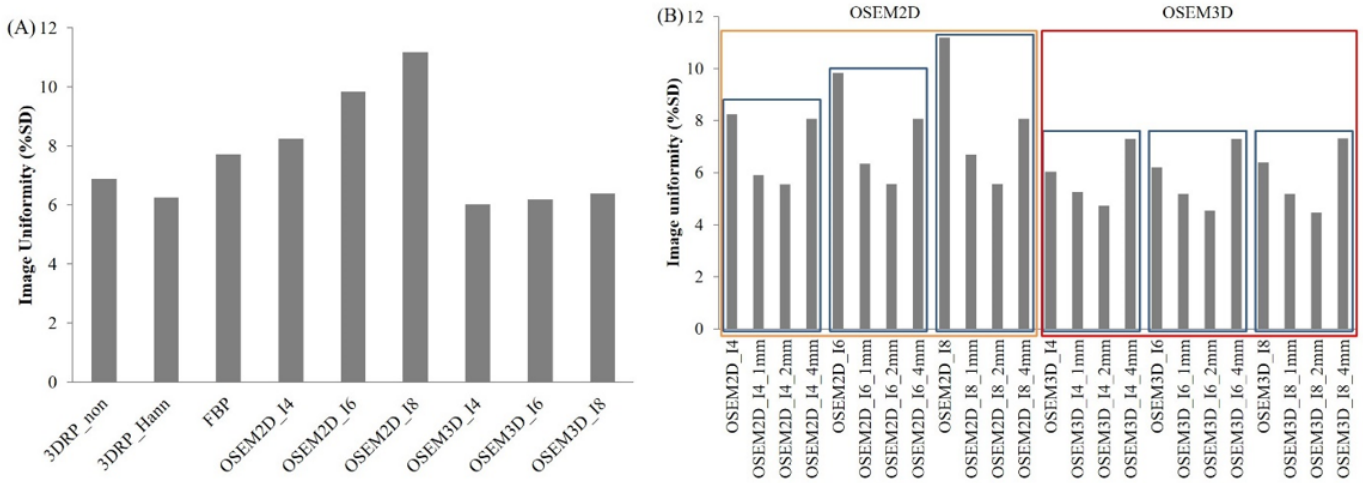

Figure 3. The uniformity of images was compared by %SD in uniformity area of the NEMA NU-4 mouse image quality phantom. (**A**) The uniformity of 3DRP and OSEM3D was higher than that of FBP. The uniformity of OSEM2D was lower than that of FBP. In iterative reconstruction methods, image uniformity decreased with increasing number of iterations. (**B**) In the iterative reconstruction methods (OSEM2D and OSEM3D), the image uniformities were compared by post-Gaussian filter effect. The image uniformity increased with the use of a Gaussian filter of 1 or 2 mm. However, the image uniformity decreased with the use of a Gaussian filter of 4 mm.

3.4. Spillover Ratio (SOR)

The SOR (Equation (3)) was estimated as mean of uniform area to the mean of water or air area (Figure 4). The SOR in water (0.205 ± 0.021) was significantly higher than that in air (Figure 4A) (0.119 ± 0.018) in the reconstruction methods without Gaussian post-filtering ($p < 0.001$). In the iterative methods, the SOR slowly decreased with increasing iteration numbers. The SOR rapidly increased with increasing Gaussian filter size (Figure 4B). The SOR values of the 1, 2, and 3 mm Gaussian filtering compared with nonfiltering

increased approximately 1.04, 1.19, and 1.74 times in the OSEM2D reconstruction method and about 1.04, 1.21, and 1.80 times in the OSEM3D reconstruction method.

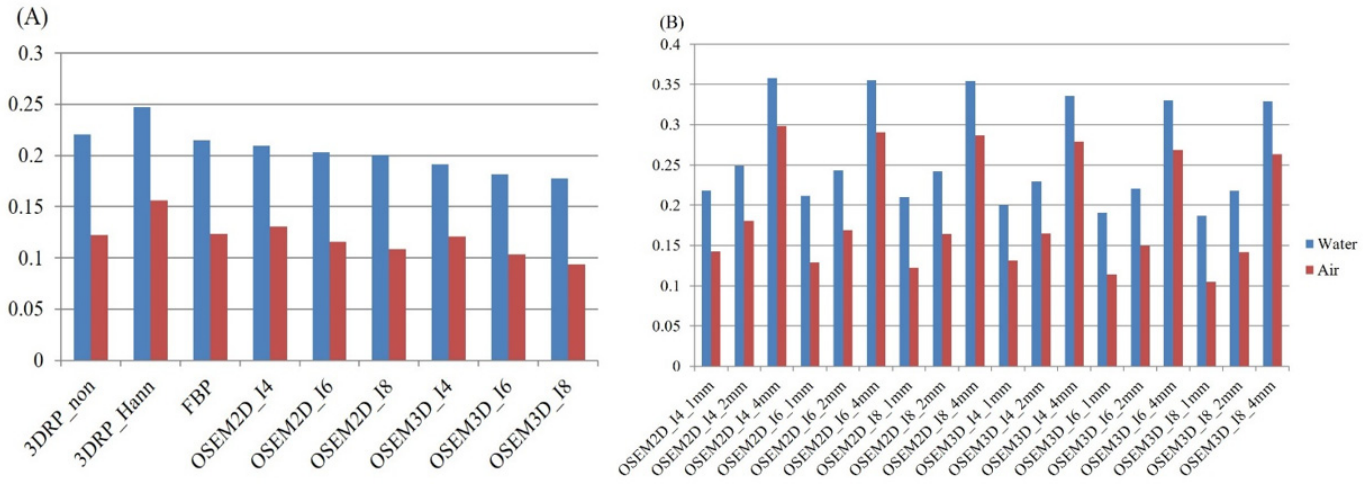

Figure 4. The spillover ratio (SOR) was estimated as the mean of uniform area to the mean of water or air area. (**A**) The SOR in water was significantly higher than that in air in the reconstruction methods without Gaussian post-filtering ($p < 0.001$). (**B**) In the iterative methods, SOR decreased with increasing iteration number and increased with increasing Gaussian filter size ($p < 0.05$).

PSNR was calculated on the hot rod of 5 mm diameter. The higher PSNR was 22.44 dB in OSEM3D_I8 and the lowest PSNR was 19.32 dB in OSEM2D_I8. The PSNR values of other methods (3DRP, 3DRP_Hann, FBP, OSEM2D_I4, OSEM2D_I6, OSEM3D_I4, and OSEM3D_I6) were 19.68, 19.78, 20.52, 19.79, 19.49, 19.77, and 21.48 dB, respectively.

4. Discussion

We confirmed data credibility by comparison to previously reported data [6]. Our recovery coefficient values reconstructed to FBP were similar to those reconstructed to FBP in another study.

In iterative reconstruction methods, image uniformity decreased depending on the number of iterations, because image noise increased along with number of iterations (Figure 3A). However, the increased range of OSEM3D was lower than that of OSEM2D. This disadvantage could be overcome by Gaussian filtering (Figure 3B). However, a filter size larger than 2 mm resulted in image distortion due to high blurring. The reconstruction time of 3DRP was the longest (10:04:40, 43 frames, Table 1).

Table 1. Reconstruction times (hh:mm:ss) measured by embedded Inveon computer.

Reconstruction Methods	Total Time	Average Time (Per Frame)
3DRP_non	10:04:40	00:14:03
3DRP_Hann	10:04:46	00:14:03
FBP	00:09:49	00:00:13
OSEM2D_I4	00:11:33	00:00:16
OSEM2D_I6	00:13:02	00:00:18
OSEM2D_I8	00:16:10	00:00:22
OSEM3D_I4	04:08:07	00:05:46
OSEM3D_I6	05:54:34	00:08:14
OSEM3D_I8	07:41:45	00:10:44

The SOR effect in water was stronger than that in air. The SOR effect of the iterative reconstruction methods trended lower than that in the analytic reconstruction methods. However, it increased with increased iteration numbers and post-filtering was crucial for myocardial blood flow (MBF) evaluation in cardiac PET imaging.

In the PET images, the reconstruction method and post-filtering affected the image quality, and activity correction of the target (tumor, brain, or heart) was positively necessary for accurate analysis. Tumor activity should be corrected by the RC value of actual tumor size. In cardiac PET image analysis, the TAC of blood pool and myocardium needs correction because of the spillover effect from myocardium to blood pool or from blood pool to myocardium.

A limitation of this study is that we did not compare new, recently developed reconstruction algorithms. If the reconstruction algorithms of the Inveon system are updated, we will perform further study.

5. Conclusions

Image accuracy of the OSEM2D was higher than those of other reconstruction methods. The overcompensated recovery coefficients filtered by the 2 mm Gaussian filter resembled the values of FBP. The image uniformity of OSEM3D was higher than those of other reconstruction methods. The SOR values of the 3DRP and FBP reconstruction methods were higher than that of iterative reconstruction methods. The reconstruction time (14 min) of 3DRP was longer than those of other reconstruction methods.

In Inveon microPET imaging, iterative reconstruction methods provided better image quality for tumors smaller than 3 mm. For tumors bigger than 3 mm, the FBP, 3DRP, and OSEM2D reconstruction methods without post-filtering showed better results. The OSEM3D reconstruction method with 1 mm Gaussian post-filtering enhanced the image accuracy and image quality. To conclude, we need to select the appropriate reconstruction method and post-filtering for correct image analysis or interpretation, because post-filtering enhances image uniformity but impairs image accuracy.

In the myocardial blood flow (MBF) measurement using dynamic PET image, Patlak analysis with recovery coefficients is widely used. Our future work is on validation of Patlak analysis with recovery coefficients and the development of the MBF measurement program using Patlak analysis.

Author Contributions: Conceptualization, B.-i.L.; Data curation, H.-S.K.; Formal analysis, H.-S.K.; Methodology, B.-i.L.; Visualization, J.-S.A.; Writing—Original draft, H.-S.K. and J.-S.A.; Writing—Review & editing, H.-S.K. and J.-S.A. All authors have read and agreed to the published version of the manuscript.

Funding: This research was funded by Basic Science Research Program of the National Research Foundation (NRF) of Korea (NRF-2018R1D1A1B07049322) and by a National Research Foundation of Korea (NRF) grant funded by the Korean government (MSIT) (NRF- 2017M3A9E2056373).

Institutional Review Board Statement: Not applicable.

Informed Consent Statement: Not applicable.

Data Availability Statement: Data is contained within the article.

Acknowledgments: This study was supported by a grant from the Basic Science Research Program of the National Research Foundation (NRF) of Korea (NRF-2018R1D1A1B07049322) and by a National Research Foundation of Korea (NRF) grant funded by the Korean government (MSIT) (NRF-2017M3A9E2056373).

Conflicts of Interest: The authors declare no conflict of interest.

References

1. Di Martino, F.; Barca, P.; Bortoli, E.; Giuliano, A.; Volterrani, D. Correction for the Partial Volume Effects (PVE) in Nuclear Medicine Imaging: A Post-Reconstruction Analytic Method. *Appl. Sci.* **2021**, *11*, 6460. [CrossRef]
2. Jomaa, H.; Mabrouk, R.; Khlifa, N. Validation of iterative multi-resolution method for partial volume correction and quantification improvement in PET image. *Biomed. Signal Process. Control.* **2020**, *60*, 101954. [CrossRef]
3. Lu, Y.; Toyonaga, T.; Naganawa, M.; Gallezot, J.D.; Chen, M.K.; Mecca, A.P.; van Dyck, C.H.; Carson, R.E. Partial volume correction analysis for ^{11}C-UCB-J PET studies of Alzheimer's disease. *NeuroImage* **2021**, *238*, 118248. [CrossRef]

4. Akerele, M.I.; Karakatsanis, N.A.; Deidda, D.; Cal-Gonzalez, J.; Forsythe, R.O.; Dweck, M.R.; Syed, M.; Newby, D.E.; Aykroyd, R.G.; Sourbron, S.; et al. Comparison of Correction Techniques for the Spillin Effect in Emission Tomography. *IEEE Trans. Radiat. Plasma Med. Sci.* **2020**, *4*, 422–432. [CrossRef] [PubMed]
5. Gould, K.L.; Bui, L.; Kitkungvan, D.; Pan, T.; Roby, A.E.; Nguyen, T.T.; Johnson, N.P. Pitfalls in quantitative myocardial PET perfusion I: Myocardial partial volume correction. *J. Nucl. Cardiol.* **2020**, *27*, 386. [CrossRef] [PubMed]
6. Bao, Q.; Newport, D.; Chen, M.; Stout, D.B.; Chatziioannou, A.F. Performance evaluation of the inveon dedicated PET preclinical tomograph based on the NEMA NU-4 standards. *J. Nucl. Med.* **2009**, *50*, 401–408. [CrossRef] [PubMed]
7. Disselhorst, J.A.; Brom, M.; Laverman, P.; Slump, C.H.; Boerman, O.C.; Oyen, W.J.; Gotthardt, M.; Visser, E.P. Image-quality assessment for several positron emitters using the NEMA NU 4-2008 standards in the Siemens Inveon small-animal PET scanner. *J. Nucl. Med.* **2010**, *51*, 610–617. [CrossRef]
8. Prasad, R.; Ratib, O.; Zaidi, H. NEMA NU-04-based performance characteristics of the LabPET-8 small animal PET scanner. *Phys. Med. Biol.* **2011**, *56*, 6649–6664. [CrossRef] [PubMed]
9. Goertzen, A.L.; Bao, Q.; Bergeron, M.; Blankemeyer, E.; Blinder, S.; Cañadas, M.; Chatziioannou, A.F.; Dinelle, K.; Elhami, E.; Jans, H.-S.; et al. NEMA NU 4-2008 comparison of preclinical PET imaging systems. *J. Nucl. Med.* **2012**, *53*, 1300–1309. [CrossRef] [PubMed]
10. Gu, Z.; Taschereau, R.; Vu, N.T.; Wang, H.; Prout, D.L.; Silverman, R.W.; Bai, B.; Stout, D.B.; E Phelps, M.; Chatziioannou, A.F. NEMA NU-4 performance evaluation of PETbox4, a high sensitivity dedicated PET preclinical tomograph. *Phys. Med. Biol.* **2013**, *58*, 3791–3814. [CrossRef] [PubMed]
11. Liu, Q.; Li, C.; Liu, J.; Krish, K.; Fu, X.; Zhao, J.; Chen, J.C. Performance evaluation of a small-animal PET/CT system based on NEMA NU 4–2008 standards. *Med. Phys.* **2021**. [CrossRef] [PubMed]
12. Manzo, M.; Pellino, S. Fighting Together against the Pandemic: Learning Multiple Models on Tomography Images for COVID-19 Diagnosis. *AI* **2021**, *2*, 261–273. [CrossRef]
13. Gao, J.; Liu, Q.; Zhou, C.; Zhang, W.; Wan, Q.; Hu, C.; Gu, Z.; Liang, D.; Liu, X.; Yang, Y.; et al. An improved patch-based regularization method for PET image reconstruction. *Quant. Imaging Med. Surg.* **2021**, *11*, 556. [CrossRef] [PubMed]
14. Yu, A.R.; Kim, J.S.; Kang, J.H.; Lim, S.M. Comparison of reconstruction methods and quantitative accuracy in Siemens Inveon PET scanner. *J. Instrum.* **2015**, *10*, P04001. [CrossRef]
15. Lubberink, M.; Boellaard, R.; van der Weerdt, A.P.; Visser, F.C.; Lammertsma, A.A. Quantitative comparison of analytic and iterative reconstruction methods in 2- and 3-dimensional dynamic cardiac 18F-FDG PET. *J. Nucl. Med.* **2004**, *45*, 2008–2015. [PubMed]
16. Søndergaard, H.M.; Madsen, M.M.; Boisen, K.; Bøttcher, M.; Schmitz, O.; Nielsen, T.T.; Bøtker, H.E.; Hansen, S.B. Evaluation of iterative reconstruction (OSEM) versus filtered back-projection for the assessment of myocardial glucose uptake and myocardial perfusion using dynamic PET. *Eur. J. Nucl. Med. Mol. Imaging* **2007**, *34*, 320–329. [CrossRef] [PubMed]
17. Kim, H.S.; Lee, B.I.; Han Kim, J.; Bom, H.S.; Kim, D.Y.; Min, J.J. Comparison of Reconstruction Methods in a Small Animal Cardiac Positron Emission Tomography Study Using a ^{18}F-Labeled Myocardial Agent, [^{18}F] FPTP. *Iran J. Radiol.* **2017**, *14*, e13463. [CrossRef]